Solution Structure of a Novel Disintegrin, Salmosin, from *Agkistrondon halys* Venom[†,‡]

Joon Shin,[§,||] Sung-Yu Hong,[§] Kwanghoe Chung,[⊥] Incheol Kang,[▽] Yangsoo Jang,[⊥] Doo-sik Kim,[§] and Weontae Lee*[,§,||]

Department of Biochemistry and HTSD-NMR Laboratory, College of Science, Yonsei University, Seoul 120-740, Korea, Cardiovascular Research Institute and BK21 Project for Medical Sciences, Yonsei University College of Medicine, Seoul 120-752, Korea, and Department of Oncology, Graduate School of East-West Medical Science, Kyunghee University, Seoul 130-701, Korea

Received January 31, 2003; Revised Manuscript Received July 10, 2003

ABSTRACT: Disintegrins are potent inhibitors of both platelet aggregation and integrin-dependent cell adhesion. A new disintegrin, salmosin, isolated from the venom of the Korean snake *Agkistrodon halys brevicaudus*, has been characterized by mass spectrometry and NMR spectroscopy, and its in vitro biological activity has been assessed. The IC_{50} value of the purified salmosin was determined to be 2.2 nM in an assay for the inhibition of glycoprotein IIb-IIIa/fibrinogen interaction. Salmosin also inhibited the bovine capillary endothelial cell proliferation induced by bFGF in a dose-dependent manner. The NMR solution structures were well converged with a root-mean-square deviation of 0.76 Å for backbone atoms among the 20 lowest energy structures, except for the arginylglycylaspartic acid (RGD) loop. The structure revealed that the conserved RGD motif with an unusual finger shape is distal from the rigid core of the C-terminal domain. Furthermore, even though the RGD motif did not interact with the hydrophobic core of the protein, it was stabilized by a network of molecular contacts through a small antiparallel β-sheet comprising residues of Ile46−Ala50 and Asp54−Tyr58. Last, the electrostatic charge distribution on the surface of salmosin differs dramatically from that of other disintegrin proteins in that there is a cluster of negatively charged residues in close proximity to the RGD loop.

Salmosin, a component of the venom of the Korean snake *Agkistrodon halys brevicaudus*, belongs to a family of cysteine-rich proteins derived from the venom of various vipers (*1*−*3*). The primary sequence of salmosin represents a novel family of small- to medium-sized disintegrins with molecular masses of 5400−9000 Da (Figure 1). It was recently reported that a new disintegrin, salmosin, significantly inhibited bovine capillary endothelial cell proliferation, induced by a basic fibroblast growth factor without affecting normal cell growth at all (*1*, *3*).

Disintegrins containing the Arg-Gly-Asp (RGD[1]) motif bind to integrin receptors on the surface of both blood platelets and other cells, and their biological roles have been studied extensively (*4*−*13*). The tripeptide RGD sequence has also been shown to act as the principal element in all adhesive proteins for the recognition of integrin-type surface receptors. These molecules are involved in a variety of biochemical processes including platelet aggregation, cell migration, metastasis, tissue remodeling, osteoclast activity, and regulation of embryogenesis (*1*, *2*, *14*). The snake venom proteins are also potent inhibitors of fibrinogen activity by virtue of their ability to bind to the platelet glycoprotein IIb-IIIa (GP IIb-IIIa) integrin, which inhibits aggregation of activated platelets (*6*). Since platelet aggregation is a key step in thrombus formation, therapeutic intervention at this level could be of importance for the treatment of diseases related to arterial thrombosis.

It has been reported that other adhesive proteins including fibrinogen, fibronectin, vitronectin, and von Willebrand factor, can bind to GP IIb-IIIa (*12*). The high abundance of fibrinogen in blood plasma leads us to suggest that it might play an important role in platelet aggregation. A number of structure−function studies for snake venom disintegrins and short RGD peptide models have shown that the biological activities of the small RGD-containing peptides are approximately 3 orders of magnitude lower than those of the native disintegrin proteins (*15*−*19*). Therefore, the overall

[†] This study was supported by the Ministry of Science and Technology of Korea/Korea Science and Engineering Foundation through the NRL program of MOST NRDP (Grant M1-0203-00-0020) (W.L.) and G7 Grant 00-G-08-01-A-04 from the Ministry of Science and Technology (K.C.).

[‡] The atomic coordinates for 20 final simulated annealing structures and the restrained-energy minimized average structure together with experimental restraints and NMR chemical shifts have been deposited in the Protein Data Bank (access code 1L3X) and BMRB (accession code 5346).

* To whom correspondence should be addressed. Phone: 82-2-2123-2706. Fax: 82-2-363-2706. E-mail: wlee@spin.yonsei.ac.kr.

[§] Department of Biochemistry, Yonsei University.

[||] HTSD-NMR Laboratory, Yonsei University.

[⊥] Yonsei University College of Medicine.

[▽] Kyunghee University.

[1] Abbreviations: BCE, bovine capillary endothelial; RGD, arginylglycylaspartic acid; MALDI-TOF, matrix-assisted laser desorption ionization time of flight; NMR, nuclear magnetic resonance; 1D, one-dimensional; 2D, two-dimensional; NOESY, nuclear Overhauser effect spectroscopy; TOCSY, total correlated spectroscopy; DQF-COSY, double-quantum-filtered correlated spectroscopy; SA, simulated annealing.

10.1021/bi0300276 CCC: $25.00
Published on Web 11/20/2003

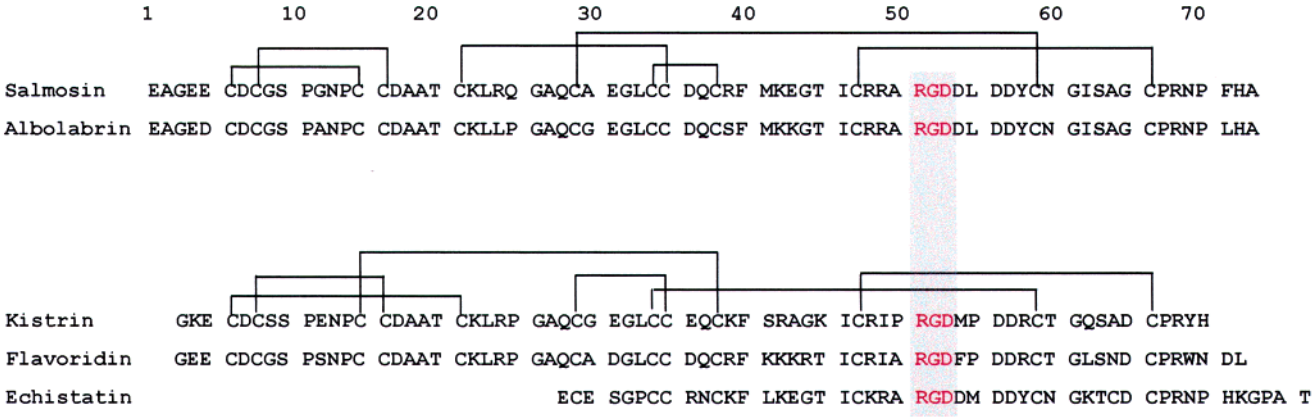

FIGURE 1: Amino acid sequences of the disintegrin family. The solid lines indicate the location of disulfide bonds.

conformation of full-length salmosin is deemed to be of importance for biological activity. In this paper, we present the NMR solution structure of salmosin and a detailed structure−function analysis of this novel disintegrin.

EXPERIMENTAL PROCEDURES

Sample Preparation for Biological Assay. Platelet GP IIb-IIIa was prepared using the method described by Pytela et al. (*20*) and stored frozen (−80 °C) in TACTS (20 mM Tris−Cl, pH 7.5/0.02% NaN_3/2 mM $CaCl_2$/0.05% Tween 20/150 mM NaCl). The pentapeptide Gly-Arg-Gly-Asp-Ser-Pro (GRGDSP) for biological assay was synthesized using fmoc chemistry and purified on a reversed-phase C18 column using a 0.1% trifluoroacetic acid/acetonitrile gradient. The primary culture of bovine capillary endothelial (BCE) cells was obtained from bovine adrenal tissue (*21*).

Fibrinogen/GP IIb-IIIa ELISA. Fibrinogen/GP IIb-IIIa ELISA was performed by a modified method of Nachman and Leung (*22*). Microtiter plates were coated with purified human fibrinogen (10 g/mL). After blockage with 1% bovine serum albumin in TACTS solution for 1 h, both the protein and synthetic peptide were loaded immediately onto the washed plate by addition of purified GP IIb-IIIa (40 mg/mL) in TACTS containing 0.5% bovine serum albumin. After incubation for 2 h, the plate was washed again and mouse anti-human GP IIIa antibody was added. After an additional hour of incubation and washing, goat anti-mouse IgG conjugated with horseradish peroxidase was treated. The plate was further washed prior to developing. Finally, the plate was incubated for 10 min to allow for development. The reaction procedure was controlled with 3 M HCl and the absorbance measured at 492 nm.

BCE Cell Proliferation Assay. The cells were maintained in Dulbecco's minimum essential medium (DMEM) containing 3 ng/mL basic FGF supplemented with 10% fetal calf serum. The proliferation assay was performed as described previously (*23*). The BCE cells were plated onto 24 gelatinized culture plates and incubated at 37 °C in 5% CO_2 for 24 h. After immediate incubation, the cells were treated with salmosin by replacing the media with 0.25 mL of DMEM containing 5% fetal calf serum. After incubation for 20 min, the cells were treated with bFGF (1 ng/mL) dissolved in the media. After an additional 72 h of incubation, the cells were treated with trypsin and counted.

Identification of Disulfide Bonds. Salmosin (2 mg/mL in 100 mM NH_4HCO_3, pH 8.0) was digested with TPCK-trypsin (Sigma-Aldrich Chemical Co.) at a protein:enzyme ratio of 50:1 (w/w) by incubation for 18 h at 37 °C. The trypsin digests were heat deactivated at 100 °C for 5 min, and porcine pancreatic elastase (Sigma-Aldrich) was titrated into the solution, yielding a final protein-to-enzyme ratio of up to 25:1 (w/w). The enzyme mixture was further incubated for 12 h at 37 °C. Elastase was heat deactivated again by incubation at 100 °C for 5 min. Finally, the remaining salt was removed by a vacuum dryer. The molecular mass of the digest products was determined using a Voager DE-STR MALDI-TOF mass spectrometer (PerSeptive Biosystems, Inc).

Sample Preparations for NMR Spectroscopy. Salmosin was purified from the *A. halys brevicaudus* snake venom as previously reported (*3*). The sample for NMR measurements was prepared by dissolving the protein in 90% H_2O/10% D_2O or 99.9% D_2O at pH values of 4.0−7.4 in a 50 mM sodium phosphate buffer. The concentration of the NMR samples was approximately 2−4 mM.

NMR Spectroscopy. NMR experiments were performed on Bruker DRX600 and DRX500 spectrometers equipped with a triple-resonance probe head and a triple-axis gradient coil. All NMR data were collected at temperatures of 10−37 °C to resolve resonance overlap. The strong solvent resonance was suppressed by water-gated pulse sequences combined with pulsed field gradients (PFGs). Nuclear Overhauser effect spectroscopy (NOESY) experiments were performed with mixing times of 50−400 ms. Total correlation spectroscopy (TOCSY) (*24*) data were recorded in both H_2O and D_2O solutions with mixing times of 39.3 and 69.7 ms, using MLEV17 spin lock pulses (*25*). Vicinal coupling constants were determined using the double-quantum-filtered COSY experiment (*26*). All data were recorded in the phase-sensitive mode using the time-proportional phase increment (TPPI) method (*27*), with 2048 data points in the t_2 domain and 256 points in the t_1 domain. Slowly exchanging amide protons were identified by lyophilization of a fully protonated sample in H_2O solution to dryness, resuspension in a 99.99% D_2O solution, and immediate acquisition of a series of 2D NOESY spectra (*28*). The DQF-COSY data were processed to 8192 × 1024 data matrixes to obtain maximum digital resolution for coupling constant measurements.

All NMR data were processed using Bruker XWIN-NMR (Bruker Instruments) software on a SGI Indigo^2 workstation and analyzed by Sparky 3.60 software (*29*). The proton

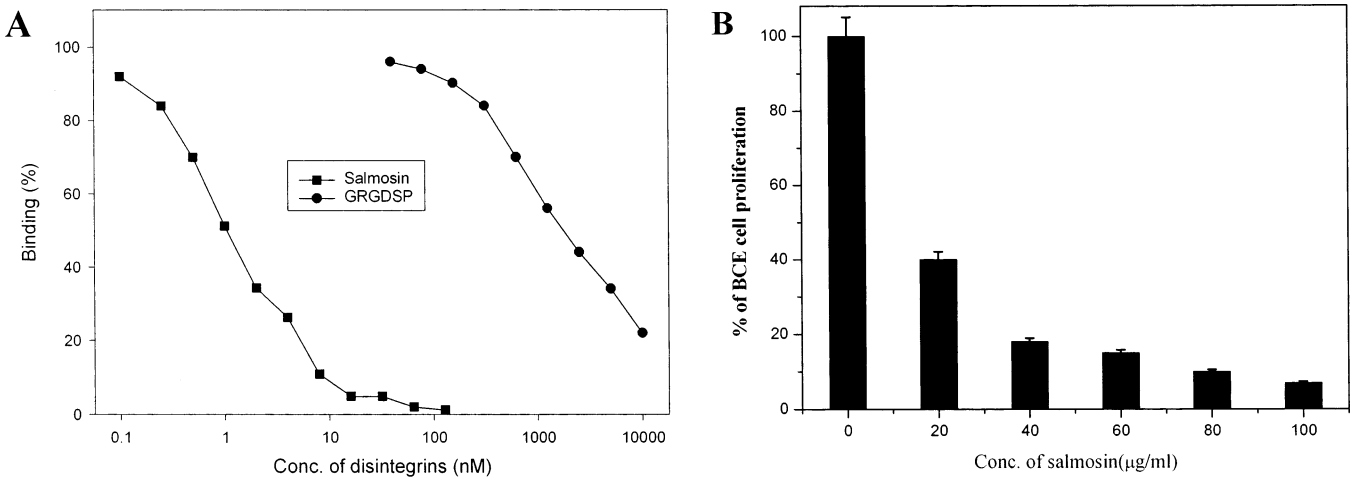

FIGURE 2: (A) Inhibition of GP IIb-IIIa binding to immobilized fibrinogen, measured by the solid-phase ELISA assay described in the Materials and Methods. Concentration is plotted on a log scale. The IC_{50} values of salmosin and GRGDSP were 2.2 nM and 4.2 μM, respectively. (B) Inhibition profile of bovine capillary endothelial cell proliferation. The BCE cells were treated with recombinant salmosin for 72 h in the presence of 1 ng/mL bFGF. The bFGF-induced proliferation assay was carried out according to the concentration of salmosin.

chemical shifts were referenced to a sodium 2,2-dimethyl-4-silapentane-1-sulfonate (DSS) internal standard.

Structure Calculations. Structure calculations were performed using CNS 1.0 (*30*) on an SGI Indigo^2 workstation. Solution structures were calculated by the hybrid distance geometry and simulated annealing (SA) protocol (*31*−*34*). The protocol used for salmosin is basically the same as previously reported (*32*), employing four stages: initial regulation and annealing to satisfy experimental constraints, regulation and refinement for the ideal geometry and constraints, a prolonged cooling procedure for final structures, and 5000 steps of energy minimization. In all of the stages except the last one, the value of K_{vdw} is slowly changed from a very low value (0.003 or 0.01) to 4.0, allowing atoms to easily pass each other during molecular dynamics.

The potential energy function consisted of covalent, repulsion, NOE, and torsion angle terms. The target functions used for NOE and torsion angle restraints were the same as those used by Driscoll et al. (*35*). A total of 1005 distance and 45 torsion angle constraints were used for structure calculations. NOE distance constraints were classified as strong (1.8−2.7 Å), medium (1.8−3.3 Å), weak (1.8−5.0 Å), or very weak (1.8−6.0 Å), on the basis of the intensities derived from the NOESY spectrum at 25 °C, pH 7.4. Corrections for pseudoatom representations were used for nonstereospecifically assigned methylene, methyl group, and tyrosine ring protons (*27*). Backbone dihedral angle restraints were derived from $^3J_{HN-H\alpha}$ coupling constants in DQF-COSY spectra in H_2O solution (35). Backbone dihedral restraints were used as $-55° \pm 45°$($^3J_{HN\alpha} < 6$ Hz) and $-120° \pm 50°$($^3J_{HN\alpha} > 8$ Hz). Each of the six disulfide bonds were represented by three distance constraints: $r_{S(i)-S(j)} = 2.0 \pm 0.1$ Å, $r_{C\beta(i)-S(j)} = 3.0 \pm 0.1$ Å, and $r_{S(i)-C\beta(j)} = 3.0 \pm 0.1$ Å. The final structures were analyzed using PROCHECK and displayed using Insight II (Biosym/Molecular Simulations, Inc.) and the MOLMOL program (*36*).

RESULTS

Antagonism of GP IIb-IIIa. The interaction of GP IIb-IIIa with immobilized fibrinogen was directly inhibited by salmosin. The specific activity of salmosin was also determined using a solid-phase inhibition assay. The typical concentration−response curves (Figure 2A) yielded an IC_{50} value of 2.2 nM for the GP IIb-IIIa/fibrinogen interaction, which is considerably stronger than that of the synthetic pentapeptide with a GRGDS sequence ($IC_{50} = 4.2$ μM). This result suggests that the structural integrity of the protein is of importance for enhancing its optimum activity.

Inhibition of BCE Cell Proliferation. We employed the BCE cell proliferation to measure the inhibition of angiogenesis, which is well established for tumor angiogenesis (*2*). Salmosin inhibited the basic FGF, induced by BCE cell proliferation in a dose-dependent manner. Half-maximal inhibition of the basic FGF, induced by BCE cell proliferation, was also observed at protein concentrations between 1 and 2 μg/mL, corresponding to activity ranges of 130−270 nM (Figure 2B).

Determination of Disulfide Bonds. The disulfide bonding pattern of salmosin was determined by combined the use of enzyme digestion and the MALDI-TOF mass spectrometry analysis. Peptide fragments, digested by both trypsin and elastase, were analyzed by MALDI-TOF mass spectrometry. The molecular masses of the digested products showed that the six disulfide-linked cysteine pairs are Cys6/Cys15, Cys8/Cys16, Cys21/Cys35, Cys29/Cys59, Cys34/Cys38, and Cys47/Cys66 (Figure 3).

Sequential Resonance Assignment. Resonance assignment was achieved by 2D DQF-COSY and TOCSY data and complemented with connectivity information for neighboring residues derived from the NOESY experiment (*38*). The spin systems of the individual amino acids were assigned by analysis of the TOCSY and DQF-COSY spectra in both H_2O and D_2O solutions. Eight glycine residues were identified from the characteristics AX spin system patterns and large active coupling constants in the DQF-COSY spectra in D_2O solution, which were confirmed by the characteristic NH/$C^{\alpha}H$ cross-peak patterns in the TOCSY spectra. Seven of the eight alanine and two threonine spin systems were easily identified by their characteristic relayed connectivities of side chains in the TOCSY spectra. Five long-chain aliphatic amino acids (two Ile and three Leu residues) were also

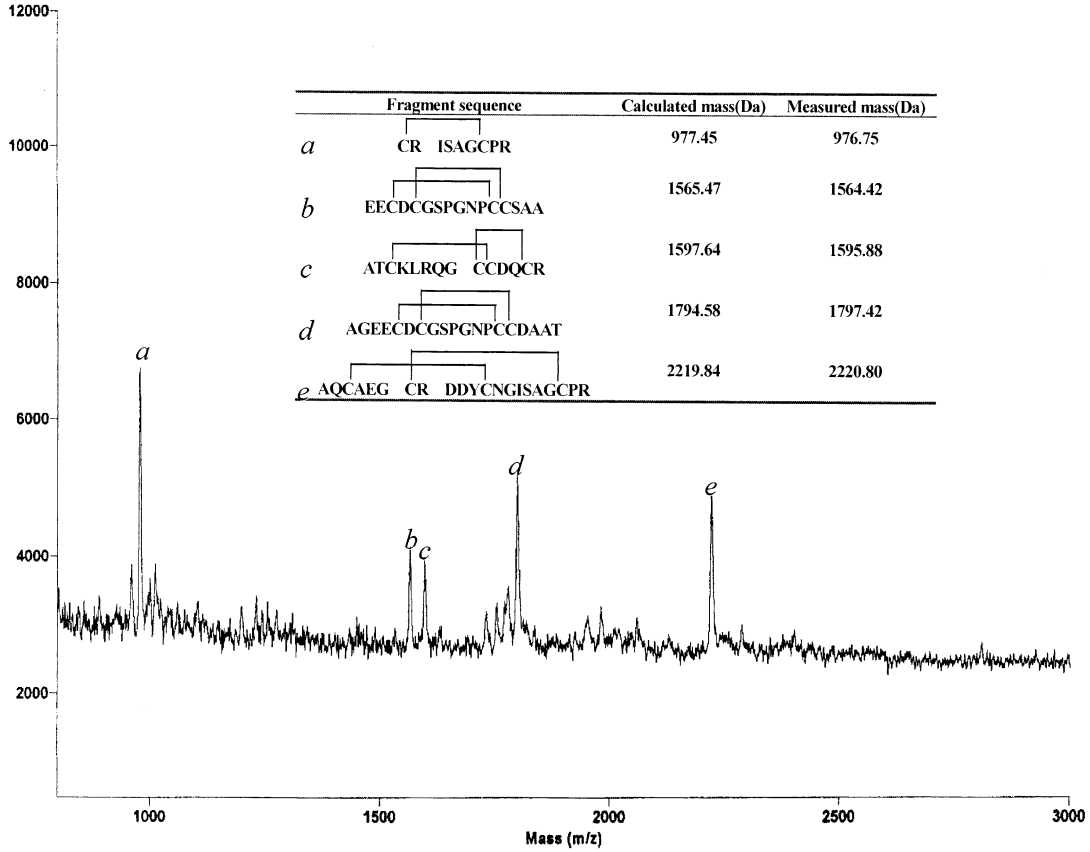

FIGURE 3: MALDI-TOF mass spectra of salmosin fragments digested by trypsin and elastase.

Table 1: Structural Statistics for the 20 Final Simulated Annealing Structures of Salmosin

	$\langle SA \rangle_k$	$\langle \overline{SA} \rangle_{kr}$
(A) RMSD from Experimental Distance Restraints (Å)		
all (1005)	0.02947	0.02801
sequential ($\|i-j\|=1$) (302)	0.02923	0.028642
medium range ($1<\|i-j\|\le 5$) (84)	0.03021	0.042049
long range ($\|i-j\|>5$) (354)	0.03565	0.042049
intraresidue (247)	0.00615	0.005513
hydrogen bond (18)	0.038755	0.019694
(B) RMSD from Experimental Dihedral Restraints (Å)		
dihedral angle restraints (45)	0.524112	0.331264
(C) Energies (kcal/mol)		
E_{NOE}	45.14 ± 4.75	38.55
E_{cdih}	1.343 ± 0.654	0.475
E_{repel}	21.87 ± 1.339	14.02
(D) Deviation from Idealized Covalent Geometry		
bonds (Å)	0.003391	0.003472
angles (deg)	0.580829	0.604315
impropers (deg)	0.421012	0.45403
(E) RMS Deviation of the Structural Segment for 20 Final $\langle SA \rangle_k$ Structures vs the $\langle \overline{SA} \rangle_k$ Structure		
backbone (Gly3−Ala50, Asp54−Pro70) (Å)	0.76 ± 0.09	
heavy atom (Gly3−Ala50, Asp54−Pro70) (Å)	1.31 ± 0.10	

assigned by their relayed connectivities in the H_2O and D_2O TOCSY spectrum. Five proline residues were assigned during the sequential resonance assignment procedure by the $d_{\alpha\delta}(i,i+1)$ NOE connectivity, combined with the characteristic coupling pattern in the TOCSY spectrum. Two phenylalanine residues, one tyrosine residue, and one histidine residue were identified as AMX spin systems and confirmed by sequential resonance assignment. Stereospecific assignments for the 19β-methylene protons were also obtained using standard procedures (*39*).

Description of the Structure. A total of 1005 distance, 45 torsion angle, 18 hydrogen bond, and 19 χ_1 angle constraints derived from NMR data were used for structure calculations (Table 1). NOE constraints were composed of 302 sequential, 84 medium-range, 354 long-range, and 247 intraresiude constraints (Figure 4). A total of 90 distance geometry (DG) structures served as starting structures for simulated annealing calculations (*31*−*34*). The 20 lowest energy structures ($\langle SA \rangle_k$) with no constraint violations greater than 0.5 Å for distances and 5° for torsion angles were selected for detailed

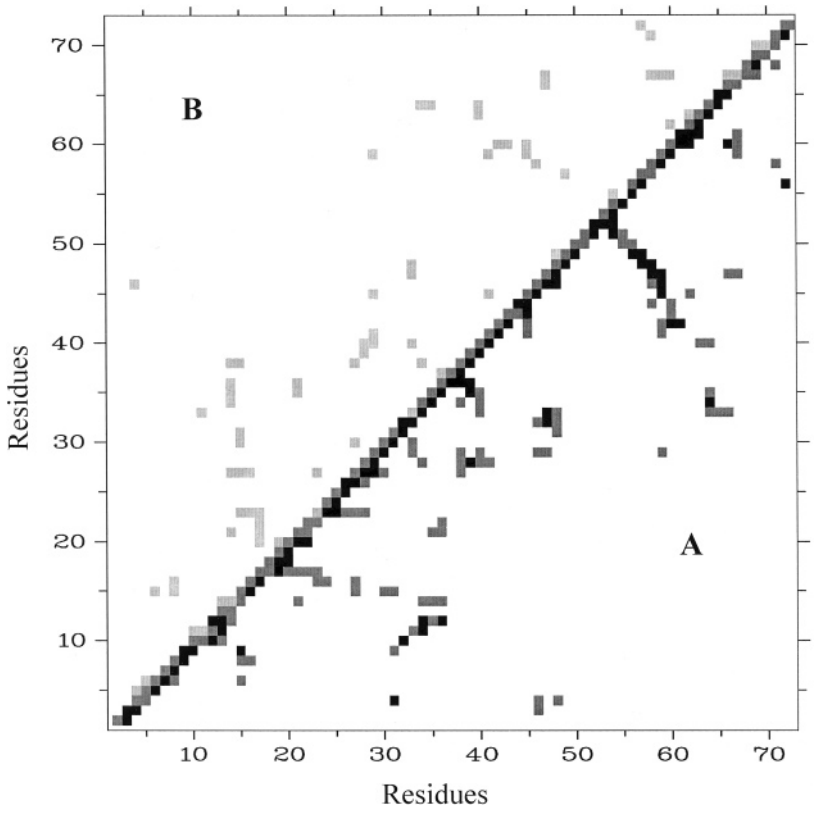

FIGURE 4: Interresidue NOE contacts for salmosin. (A) Backbone−backbone (black boxes) and side chain−side chain (gray boxes) and (B) backbone−side chain NOEs were displayed.

structural analysis. The average structure ($\langle\overline{SA}\rangle_k$) was calculated from the geometrical average of 20 $\langle SA\rangle_k$ structure coordinates and subjected to a restrained energy minimization (REM) to correct covalent bond and angle distortion. The energy and structural statistics of the final simulated annealing structures are listed in Table 1. The deviations from the idealized geometry were very small, indicating that all the final structures satisfy an ideal geometry. A best fit backbone superposition of all 20 final $\langle SA\rangle_k$ structures with respect to the $\langle\overline{SA}\rangle_{kr}$ structure is shown in (Figure 5). The final $\langle SA\rangle_k$ structures converged well with a root-mean-square deviation of 0.76 Å, for all backbone atoms, with the exception of the RGD loop region. PROCHECK analysis indicated that 95% of the residues except Cys16, Ala18, and Arg39 were distributed in the allowed region of the Ramachandran map.

Although there is no evidence of any regular secondary structure, the NOE data and amide hydrogen exchange experiments suggest that salmosin exists in a compact globular conformation. The detection of strong sequential $d_{\alpha N}(i,i+1)$ NOEs together with large values of $^3J_{HN\alpha}$ for residues in the RGD loop (R48−A50, D54−D56) indicates that this region forms a β-sheet conformation. In addition, several long-range d_{NN}, $d_{\alpha N}$, and $d_{\alpha\alpha}$ NOEs were also observed to prove a folded structure as shown in Figure 4. The six disulfide bonds were further confirmed by characteristic $d_{\beta\beta}(i,j)$ and $d_{\alpha\beta}(i,j)$ NOEs between cysteine pairs. All four prolines were determined as being in the *trans* conformation on the basis of the intensities of the $d_{\alpha\delta}(i,i+1)$ NOEs. Like other disintegrin proteins, salmosin is composed of a number of tight turns and loops (Figure 5C), and its molecular shape is well defined by a number of medium- and long-range NOEs (Figure 4). In addition, the six disulfide bonds play an important role in generating the globular structure of salmosin. The overall topology of salmosin is that of a compact globular molecule with an asymmetric charge distribution (Figure 6). The RGD loop (Arg51-Gly52-Asp53) is unstructured due to the limited number of structural constraints; however, its relative orientation is stabilized by a short β-sheet comprising residues Ile46−Ala50 and Asp54−Tyr58 as shown in Figure 5. An irregular turn, comprising residues Ile62−Gly65, enables a molecular contact between the C-terminal region and the RGD motif.

DISCUSSION

An analysis of salmosin using the the DALI program (*40*−*42*) suggested that the protein would have a topology similar to those of kistrin and flavoridin. Our solution NMR structure indicates that salmosin has a topology similar to that of kistrin, even though the two molecules have entirely different disulfide bonding patterns (Figure 1). Conversely, flavoridin has a different molecular topology, yet it bears the same disulfide bonding pattern as salmosin. Echistatin, another snake venom disintegrin, has a relatively disordered structure despite the presence of six disulfide bonds (*17*, *18*). The solution structure of albolabrin also reveals a higher proportion of loops and turns instead of regular secondary structure elements (*19*). Here we showed that salmosin is also composed of a number of tight turns and irregular loops comprising residues Gly3−Gly9, Cys15−Cys21, Lys22−Lys27, Leu33−Leu38, Gly44−Ile46, and Gly62−Gly65 and that these loops are stabilized by an array of disulfide bonds (Cys/Cys15, Cys8/Cys16, and Cys21/Cys35) (Figures 4 and 5C). Although the disintegrins share high sequence homology and in some cases similar disulfide bonding patterns, it is surprising to find that their molecular topologies are quite different. Despite these different global conformations, all

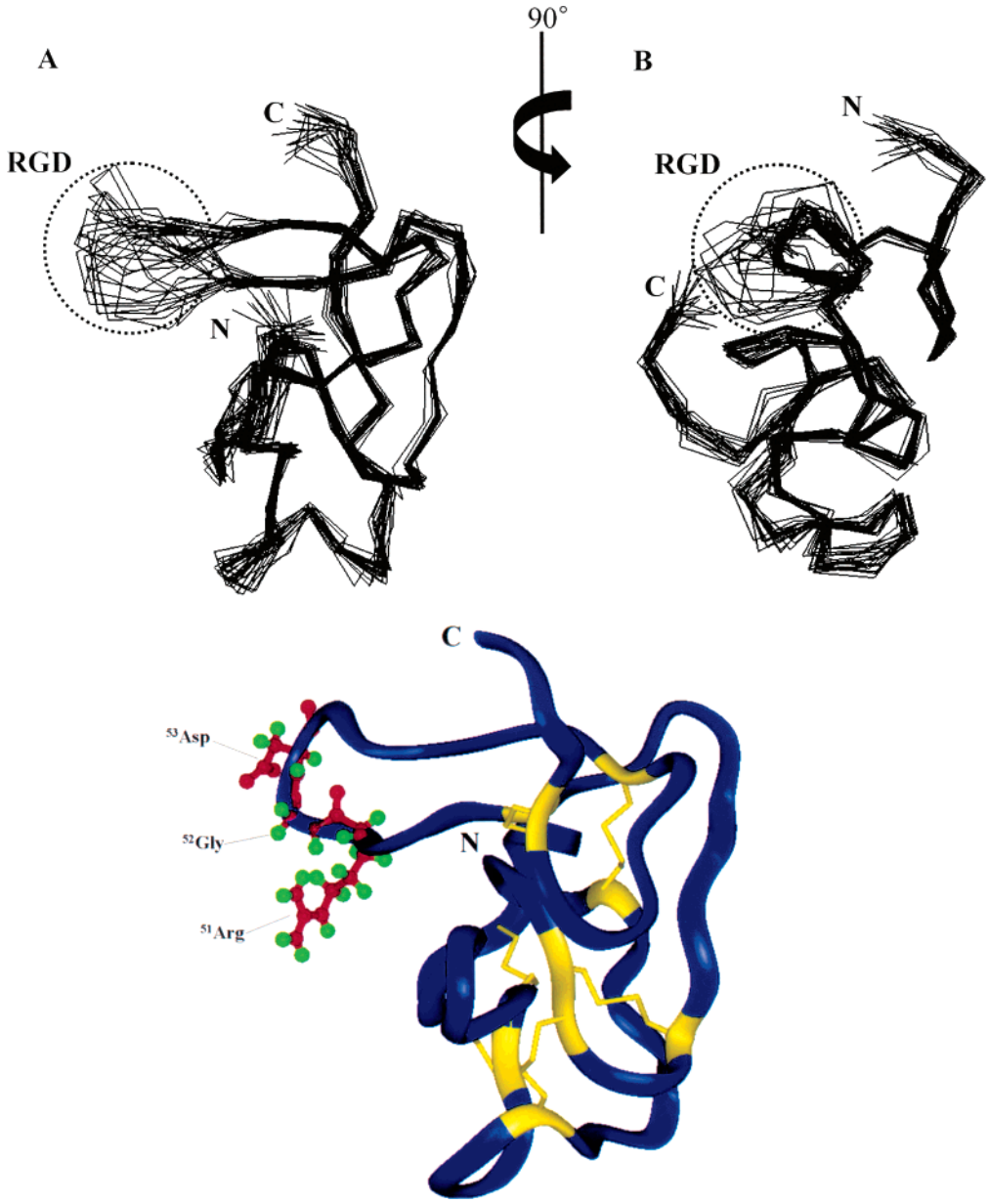

FIGURE 5: (A, B) Backbone superposition of 20 final simulated annealing structures for Gly3−Pro70. The two structures are rotated 90° about the vertical axis. (C) Ribbon diagram of the REM average structure displaying a number of turns and loops. The side chain atoms for the RGD motif and six disulfide bridges are also displayed. The figure was generated using the Insight II program.

disintegrins share a common functional motif in the solvent-exposed RGD loop, which mediates recognition of the target molecule. Given these findings, we anticipated that the three-dimensional structures of the venom-derived disintegrins could be used, at least in part, to explain receptor specificity. This hypothesis has been partly supported by a number of structure−function studies using synthetic RGD peptides (*43*−*45*).

It has been observed that cyclic RGD peptides with rigid conformations demonstrated higher biological activities than those of analogue linear, flexible peptides. Salmosin showed a 500−1000-fold increase in receptor binding as compared to that of the shorter synthetic RGD peptide (Figure 2A). This suggests that the structural topology of salmosin is an important factor in enhancing its biological activity as related to receptor binding.

Although the binding activities of disintegrin proteins are believed to originate primarily from the RGD recognition sequence, other flanking residues which interact with the RGD loop might also contribute to activity. As sequences bearing little or no homology among the disintegrins are also found in various locations throughout these molecules, such residues might also be involved in regulating specificity. The global fold and differing electrostatic surface potentials of disintegrins suggest that the unique molecular topology of disintegrin proteins containing the RGD sequence might allow its specific binding to different receptors as shown in Figure 7. Therefore, it is plausible that this conformational uniqueness among disintegrins is a major contributing factor for receptor selectivity, in addition to the RGD sequence, which is necessary for biological activity. A deletion mutant study for the echistatin protein showed that the C-terminal domain was involved in its ability to inhibit platelet aggregation (*46*). The dramatic change in inhibition activity of the deletion mutant might originate from the structural instability of the RGD adhesion motif upon deletion of

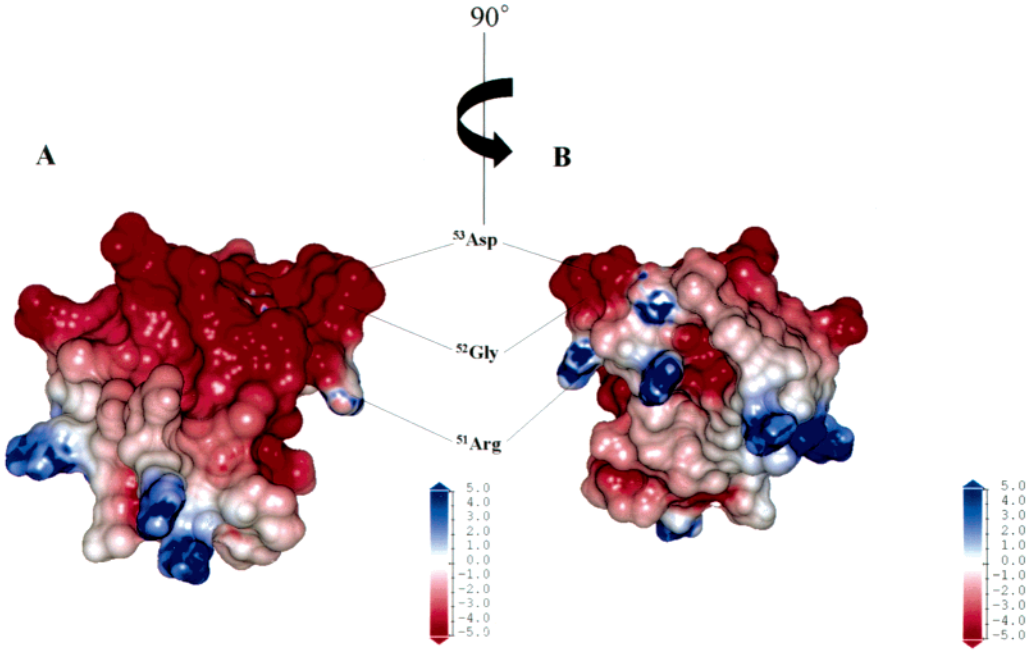

FIGURE 6: (A) Electrostatic potential surface of salmosin. The negative electrostatic potential is represented in red, the positive in blue, and the neutral in white. The RGD residues are annotated on the potential surface. (B) Backside of the salmosin rotated by 90° around the vertical axis. The Delphi program (Biosym/Molecular Simulation Inc.) generated the potential surface.

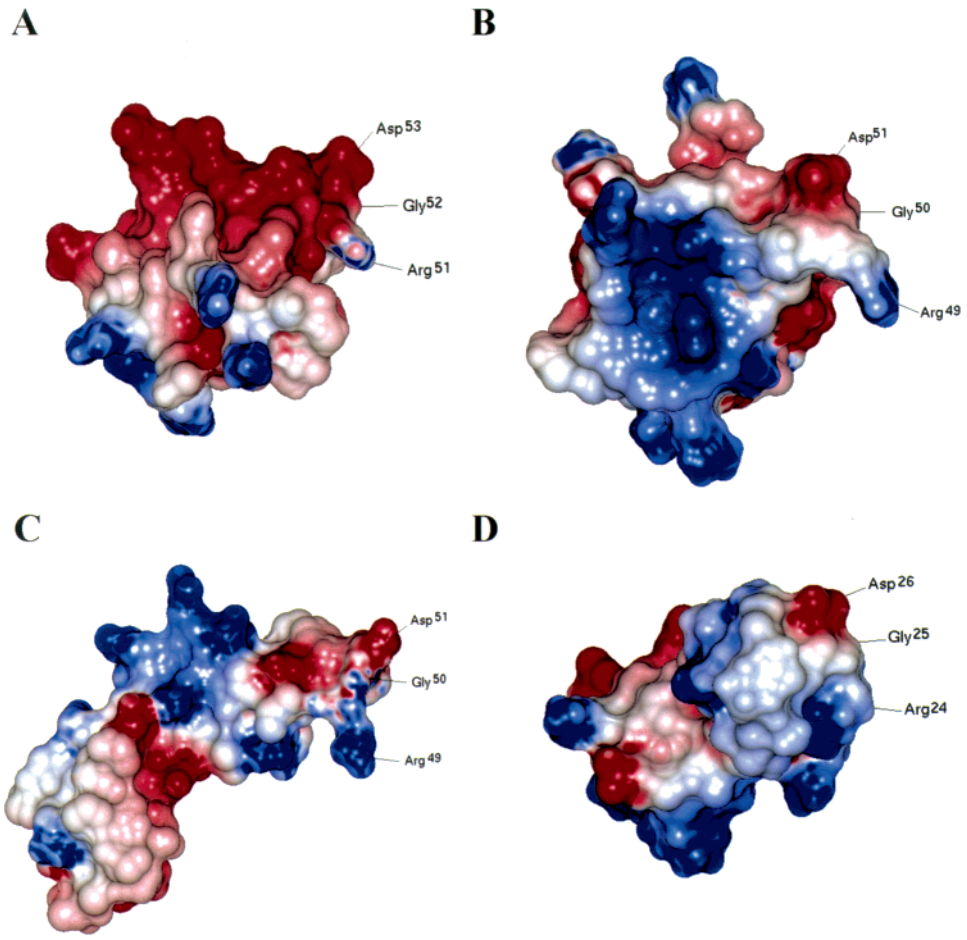

FIGURE 7: Electrostatic potential surfaces of four known disintegrin proteins: (A) salmosin, (B) kistrin (PDB code 1kst), (C) flavoridin (PDB code 1fvl) (D) echistatin (PDB code 2ech). The negative electrostatic potential is represented in red, the positive in blue, and the neutral in white. The potential surface was calculated using the Delphi program. RGD recognition motifs for different disintegrin proteins are labeled and displayed in the same orientation.

stabilizing residues within the RGD loop. Therefore, we propose that the three-dimensional topology could be one of the major contributing factors in determining the receptor affinity of snake venom disintegrins. The structural similarity

of the conserved C-terminal active sites found in echistatin, kistrin, flavoridin, and salmosin supports this hypothesis, even though three-dimensional structures of these disintegrins are quite different (Figure 7). We also note that there are dramatic differences in the electrostatic charge distributions among the four disintegrins salmosin, kistrin (PDB code 1kst), flavoridin (PDB code 1flv), and echistatin (PDB code 2ech). Salmosin has a patch of negatively charged residues proximal to the RGD loop which is not found in other disintegrins. On the other hand, a large positive charged pocket near the RGD loop was found in kistrin. Flavoridin and ecchistatin have a mixture of hydrophilic and hydrophobic residues on the protein surface. We have also shown that salmosin does not interact solely with the GP IIb-IIIa receptor but instead binds, with high affinity, to several members of the integrin receptor family (*2*, *3*). In this paper, we propose that the global fold of salmosin, in addition to the simple RGD motif, plays a critical role in mediating receptor specificity. Further studies on topics such as receptor binding mechanism using RGD peptide analogues and mutagenesis of salmosin might provide more insight into a detailed structure−function role for receptor selectivity, and this work is currently under way.

ACKNOWLEDGMENT

We thank Dr. Ayeda Ayed for critical reading of the manuscript.

SUPPORTING INFORMATION AVAILABLE

^{1}H chemical shifts, TOCSY and NOESY spectra, and connectivities of sequential and medium-range NOEs. This material is available free of charge via the Internet http://pubs.acs.org.

REFERENCES

1. Kang, I.-C., Kim, D.-S., Jang, Y., and Chung, K. H. (2000) *Biochem. Biophys. Res. Commun. 275*, 169−173.
2. Kang, I. C., Lee, Y.-D., and Kim. D.-S. (1999) *Cancer Res. 59*, 3754−3760.
3. Kang, I. C., Chung, K. H., Lee, S. J., Yoon, Y. D., Moon, H. M., and Kim, D. S (1998) *Thromb. Res. 91*, 65−73.
4. Niewiarowski, S., Mclane, M. A., Kloczewiak, M., and Stewart, G. J. (1994) *Semin. Hematol. 31*, 289−300.
5. Gan, Z. R., Gould, R. J., Jacobs, J. W., Friedman, P. A., and Polokoff, M. A. (1988) *J. Biol. Chem. 263*, 19827−19832.
6. Huang, T. F., Holt, J. C., Lukasiewicz, H., and Niewiarowski, S. (1987) *J. Biol. Chem. 262*, 16157−16163.
7. Williams, J., Rucinski, B., Holt, J., and Niewiarowski, S. (1989) *Biochemistry 28*, 661−666.
8. Dennis, M. S., Henzel, W. J., Pitti, R. M., Lipari, M. T., Napier, M. A., Deisher, T. A., Bunting, S., and Lazarus, R. A. (1990) *Proc. Natl. Acad. Sci. U.S.A. 87*, 2471−2475.
9. Scarborough, R. M., Rose, J. W., Hsu, M. A., Phillips, D. R., Frie, V. A., Campbell, A. M., Nannizzi, L., and Charo, I. F. (1991) *J. Biol. Chem. 266*, 9359−9362.
10. Huang T. F., Wu, Y. J., and Ouyang, C (1987) *Biochim. Biophys. Acta 925*, 248−257.
11. Chao, B. H., Jakubowski, J. A., Savage, B., Chow, E.P., Marzec, U. M., Harker, L.A., and Maraganore, J. N. (1989) *Proc. Natl. Acad. Sci. U.S.A. 86*, 8050−8−54.
12. Huang, T. F., Holy, J. C. Kirby, E. P., and Niewiarowski, S. (1989) *Biochemistry 28*, 661−666.
13. Musial, J., Niewiarowski, S., Rucinski, B., Stewart, G. J., Cook, J. J., Williams, J. A., and Edmunds, J. H. (1990) *Circulation 82*, 261−273.
14. Trikha, M., De Clerck, Y. A., and Markland, F. S. (1994) *Cancer Res. 54*, 4993−4998.
15. Adler, M., Lazarus, R. A., Dennis, M. S., Wagner, G. (1991) *Science 253* (5018), 445−8.
16. Senn, H., and Klaus, W. (1993) *J. Mol. Biol. 232* (3), 897−906.
17. Saudek, V., Atkinson, R. A., and Pelton, J. T. (1991) *Eur. J. Biochem. 202* (2), 323−328.
18. Saudek, V., Atkinson, R. A., Pelton, J. T. (1991) *Biochemistry 30* (30), 7369−72.
19. Smith, K. J., Jaseja, M., Lu, X., Williams, J. A., Hyde, E. I., and Trayer, I. P. (1996) *Int. J. Pept. Protein Res. 48* (3), 220−8.
20. Pytela, R., Pierschbacher, M. D., Ginsberg, M. H., Plow, E. F., and Ruoslahti, E. (1986) *Science 231*, 1559−1562.
21. Folkman J., Haudenschild, C. C., and Zetter, B. R. (1979) *Proc. Natl. Acad. Sci. U.S.A. 76*, 5217−5221.
22. Nachman, R. L., and Leung, L. L. K. (1982) *J. Clin. Invest. 69*, 263−269.
23. O'Reilly, M. S., Holmgren, L., Chen, C., Rosenthal, R. A., Moses, M., Lane, W. S., Cao, Y., Sage, E. H., and Folkman, J. (1994) *Cell 79*, 315−328.
24. Davis, D. G., and Bax, A. (1985) *J. Am. Chem. Soc. 107*, 2820−2821.
25. Bax, A., and Davis, D. G. (1985) *J. Magn. Reson. 65*, 355−360.
26. Rance, M., Soerensen, O. W., Bodehausen, G., Wagner, G., Ernst, R. R., and Wuthrich, K. (1983) *Biochem. Biophys. Res. Commun. 117*, 479−485.
27. Wuthrich, K., Billeter, M., and Braun, W. (1983) *J. Mol. Biol. 169*, 949−961.
28. Jeener, J., Meier, B. H., Bachman, P., and Ernst, R. R. (1979) *J. Chem. Phys. 71*, 4546−4553.
29. Goddard, T. D., and Kneller, D. G. SPARKY 3, University of California, San Francisco.
30. Brunger, A. T., Adams, P. D, Clore, G. M., Delano, W. L., Gros, P., Grosse-Kunstlev, R. W., Jiang, J. S., Kuszewski, J. Nilges M., Pannu, N. S., Read, R. J., Rice, L. M., Simonson, T., and Warren, G. L. (1998) *Acta Crystallogr., D 54*, 905−921.
31. Nilges, M., Clore, G. M., and Gronenborn, A. M. (1988) *FEBS Lett. 229*, 317−324.
32. Lee, W., Moore, C. H., Watt, D. D., and Krishna, N. R. (1994) *Eur. J. Biochem. 218*, 89−95.
33. Nilges, M., Gronenborn, A. M., Brunger, A. T., and Clore, G. M. (1988c) *Protein Eng. 2*, 27−38.
34. Nilges, M. (1993) *Proteins 17*, 297−309.
35. Driscoll, P. C., Gronenborn, A. M., Beress, L., and Clore, G. M. (1989) *Biochemistry 28*, 2188−2198.
36. Koradi, R., Billeter, M., and Wüthrich, K. (1996) *J. Mol. Graphics 14*, 51−55.
37. Wagner, G., Braun, W., Havel, T. F., Schaumann, T., Go, N., and Wuthrich, K. (1987) *J. Mol. Biol. 196*, 611−639.
38. Wuthrich, K. (1986) *NMR of proteins and nucleic acids*, Wiley, New York.
39. Guntert, P., Braun W., Billeter, M., Wuthrich, K. (1989) *J. Am. Chem. Soc. 111*, 3997−4004.
40. Holm, L., Sander, C. (1998) *Nucleic Acids Res. 26* (1), 316−319.
41. Holm, L., and Sander, C. (1997) *Nucleic Acids Res. 25* (1), 231−234.
42. Dietmann, S., Park, J., Notredame, C., Heger, A., Lappe, M., and Holm, L. (2001) *Nucleic Acids Res. 29* (1), 55−57.
43. Aumailley, M., Gurrath, M., Muller, G., Calvaete, J., Timple, R., and Kessler, H. (1991) *FEBS Lett. 291*, 50−54.
44. Bogusky, M. J., Naylor, S. M., Pitzenberer, S. M., Nutt. R. F., Brady, S. F., Colton, C. D., Sisko, J. T., Anderson, P. S., and Veber, D. F. (1992) *Int. J. Pept. Protein Res. 39*, 63−76.
45. McDowell, R. S., and Gadek T. R. (1992) *J. Am. Chem. Soc. 114*, 9245−9253.
46. Marcinkiewicz, C., Vijay-Kumar, S., McLane M. A., and Niewiarowski, S. (1997) *Blood 90* (4), 1565−1575.

BI0300276